TM-71-2015-3

TECHNICAL MEMORANDUM

DETECTION OF LUNAR SUBSURFACE STRUCTURE BY THE ORBITAL RADAR SOUNDER

Bellcomm

BELLCOMM, INC.
955 L'ENFANT PLAZA NORTH, S.W., WASHINGTON, D.C. 20024

COVER SHEET FOR TECHNICAL MEMORANDUM

TITLE- Detection of Lunar Subsurface Structure by the Orbital Radar Sounder

TM-71-2015-3

DATE- May 12, 1971

FILING CASE NO(S)- 340

AUTHOR(S)- W. R. Sill

FILING SUBJECT(S) (ASSIGNED BY AUTHOR(S))- Orbiting Radar Sounder

ABSTRACT

One objective of the orbital Lunar Radar Sounder Experiment (Apollo 17) is to detect subsurface structure manifested by discontinuities in the depth profile of electrical properties. However, energy backscattered from the lunar surface can interfere with the detection of energy reflected from subsurface discontinuities and which has been attenuated by a double passage through the lunar subsurface.

Recent measurements of the electrical properties of Apollo 11 and 12 samples are used to calculate the expected strength of radar echos from subsurface reflectors. The subsurface echo power is then compared with the surface backscatter power. For typical lunar parameters the expected depth of detectability of a subsurface reflector is about 150 m in rock and about 1 km in soil.

BA-145A (8-68)

SEE REVERSE SIDE FOR DISTRIBUTION LIST

DISTRIBUTION

COMPLETE MEMORANDUM TO

CORRESPONDENCE FILES:

OFFICIAL FILE COPY
plus one white copy for each additional case referenced

TECHNICAL LIBRARY (4)

NASA Headquarters
R. J. Allenby - MAL
D. A. Beattie - MAL
G. F. Esenwein, Jr. - MAL
A. S. Lyman - MR
W. T. O'Bryant - MAL
F. I. Roberson - MAL
L. R. Scherer - MAL
H. J. Smith - SS

Manned Spacecraft Center
A. J. Calio - TA
P. W. Gast - TN
W. C. Panter - EE6
M. G. Simmons - TA
D. W. Strangway - TN4

Ames Research Center
W. I. Linlor - SSE

Jet Propulsion Laboratory
W. E. Brown - 183-701
R. J. Phillips - 183-501

University of Michigan
L. Porcello

University of Utah
S. H. Ward

COMPLETE MEMORANDUM TO

Bellcomm, Inc.
R. A. Bass
A. P. Boysen, Jr.
J. O. Cappellari, Jr.
F. El-Baz
D. R. Hagner
W. G. Heffron
J. J. Hibbert
N. W. Hinners
T. B. Hoekstra
M. Liwshitz
J. L. Marshall
K. E. Martersteck
J. Z. Menard
G. T. Orrok
P. E. Reynolds
P. F. Sennewald
R. V. Sperry
A. W. Starkey
J. W. Timko
A. R. Vernon
R. L. Wagner
D. B. Wood
All Members Department 2015
Central Files
Department 1024 Files
Library

ABSTRACT ONLY TO

NASA Headquarters
R. A. Petrone - MA

Bellcomm, Inc.
J. P. Downs
D. P. Ling
M. P. Wilson

BC-145 (8-64)

BELLCOMM, INC.
955 L'ENFANT PLAZA NORTH, S.W., WASHINGTON, D.C. 20024

COVER SHEET FOR TECHNICAL MEMORANDUM

TITLE – Detection of Lunar Subsurface Structure by the Orbital Radar Sounder

TM – 71-2015-3

DATE – May 12, 1971

FILING CASE NO(S) – 340

AUTHOR(S) – W. R. Sill

FILING SUBJECT(S) (ASSIGNED BY AUTHOR(S)) – Orbiting Radar Sounder

ABSTRACT

One objective of the [illegible] Radar Sounder Experiment (Apollo 17) is to detect [illegible] structure manifested by discontinuities in the [illegible] profile of electrical properties. However, [illegible] lunar [illegible]

Recent measurements of the [illegible] properties of Apollo [illegible] and 12 samples are used [illegible] the expected strength of radar echoes from subsurface [illegible]. [illegible] surface echo [illegible] is then compared [illegible] surface [illegible] scatter power. For typical lunar [illegible] the expected depth of detectability of a subsurface [illegible] is about 150 m in rock and about 1 km in soil.

SEE REVERSE SIDE FOR DISTRIBUTION LIST

Bellcomm

955 L'Enfant Plaza North, S.W.
Washington, D. C. 20024

date: May 12, 1971

to: Distribution

TM-71-2015-3

from: W. R. Sill

subject: Detection of Lunar Subsurface Structure by the Orbital Radar Sounder -- Case 340

TECHNICAL MEMORANDUM

INTRODUCTION

A primary objective of the orbital Lunar Radar Sounding Experiment is to detect subsurface structure within 1 km of the lunar surface. In principle this objective can be accomplished by the detection of the reflected energy from discontinuities in the electrical parameters of the subsurface. In practice the detection of the subsurface reflection will be limited by the presence of various sources of noise. One major source of noise is the energy backscattered from the lunar surface which, because of the finite radar beamwidth, arrives with the same time delay as the energy reflected from the subsurface. The problem is then one of detecting the subsurface echo in the presence of backscatter from the surface.

Some of the parameters of the lunar sounding radar are given in table 1 and the geometry is shown in figure 1.

TABLE 1

LUNAR RADAR SOUNDER

Orbital Altitude ∿100 km

Frequency (MHz)	150	15	5
Wavelength (m)	2	20	60
Pulse Length (μs)	7	70	200
Compressed Pulse (μs)	.07	.7	2.
Range Resolution (m)	10	100	300
Antenna	Yagi	Dipole	Dipole

Also shown in figure 1 is the relationship between the time delay t, for a subsurface reflector at a depth d, and a surface scattering point at a horizontal distance x, from the spacecraft nadir. For the depths to be probed (<1 km) the angles are small (<15°) and it is obvious that a surface element with a local slope equal to the angle of incidence (θ) will efficiently backscatter the incident wave. These angles are also small compared to the beamwidth of the antenna, and the incident power can be considered constant over the surface distances of interest here.

Lunar Backscatter

The backscatter characteristics of the lunar surface have been studied primarily by means of earth-based radar. For short pulses the observed backscattered power as a function of the angle of incidence can be fit by [Beckmann and Klemperer, 1965; Marcus, 1969]

$$P(\theta) = [\cos^4\theta + R \sin^2\theta]^{-3/2} \quad (1)$$

where

$$R = \text{roughness parameter} = 95\ \lambda^{1/3};\ \lambda \gtrsim 1 \text{ m} . \quad (2)$$

Brown [1960, 1964] has developed an expression for the quasi-specular portion of the reflected energy. His impulse response (equation 3) when convolved with the envelope of the pulse also provides an adequate fit to the observed radar data, for a roughness factor $K\lambda = .04$,

$$I(\theta) = 1-(1+K\lambda \cot\theta) \exp(-K\lambda \cot\theta). \quad (3)$$

Equation 1 is plotted in figure 2 for the wavelengths corresponding to the three frequencies of the Radar-Sounder. Also shown are some observed data at .68 and 6 m. Figure 3 shows a plot of the impulse response of equation 3 for two values of the roughness coefficient as well as a comparison of the convolution of the impulse responses for $K\lambda = .04$ with a pulse width $t_p = 12$ μs and the observed .68 m data of Evans and Pettengill (1963). Brown's [1960] study found no appreciable dependence of the roughness factor ($K\lambda$) on wavelength for wavelengths in the range from 30 cm to 1.5 m. Radar studies (λ = 30 cm) from rocket flights over desert terrain are also compatible with equation 3 and a roughness factor $K\lambda = .04$ (Brown, 1969).

Figure 4 shows the backscatter as a function of time delay for the geometry of figure 1. The impulse response (equation 3) for 3 values of the roughness coefficient is shown as well as the convolution of the impulse response with pulse lengths of 1 and 2 μs. The 2 μs pulse length is appropriate for the Radar-Sounder frequency at 5 MHZ (λ=60 m) and the 1 μs pulse for the 15 MHZ (λ=20m) frequency.

The backscatter as given by equation 1 for the geometry of figure 1 is shown in figure 5. Also shown are two curves of the backscatter from figure 4. Note that for the stated parameters the range of the backscattered powers are similar for the two theories (equations 1 and 3).

Subsurface Signals

The energy returned from the lunar subsurface is dependent on its electrical parameters. Table 2 lists the average dielectric constants measured for some Apollo 11 and 12 samples. The dielectric constant for these samples is not a strong function of frequency in the range from 10^3 to 10^7 Hz.

TABLE 2

AVERAGE DIELECTRIC CONSTANTS FOR APOLLO 11 AND 12 SAMPLES
[COLLETT AND KATSUBE, 1971]

	Fines	Breccia	Igneous (B)	Igneous (A)
K	3.5	7.5	8.5	9.0

Values for K as large as 15 have been reported by Chung et al., 1970, for some denser Apollo 11 samples. The reflection coefficient as a function of the dielectric constant contrast is shown in figure 6. For the lunar samples the typical reflection coefficients are of the order of a few tenths.

The loss tangents for lunar and terrestrial samples are given in figure 7. The lower value of tan δ for the fines relative to the rocks is probably mostly a porosity effect, the soils having a smaller density.

The attenuation of a wave propagating through a lossy medium is

$$E^2 \sim e^{-\pi d \tan \delta/\lambda} \qquad (4)$$

The power loss as a function of time delay ($t = 2d\sqrt{K}/c$) is then

$$L(db) = 27.2\ f\ t \tan \delta \qquad (5)$$

The power loss as a function of time delay and depth of a reflector is shown in figure 8. To these transmission losses there should also be added the reflection losses at the subsurface interface, i.e.,

$$\text{Reflection loss (db)} = 10[2 \log (1-R_o) + \log R_1] \qquad (6)$$

where R_o = reflection coefficient at vacuum surface interface

R_1 = reflection coefficient at subsurface interface.

From figure 6 we see that these losses are typically of the order of -10db.

Subsurface Signal to Surface Noise Ratio

The determination of the subsurface structure is dependent upon the detection of the reflection signal in the presence of surface backscatter noise. The signal to noise ratio is

$$\frac{S}{N} = \frac{\text{Subsurface Attenuation x Reflection Loss x Data Processing Gain}}{\text{Surface Backscatter}}$$

which can be calculated from Equations 1, 3, 5 and 6. The data processing gain is reported to be about +10 db (Brown, personal communication) which will cancel the typical reflection loss (-10db). The signal to noise ratio is then approximately the subsurface attenuation to backscatter ratio. The signal to noise ratio, in db, is the difference between a power loss curve (figure 8) due to attenuation and a backscatter curve (figures 4 and 5).

Figure 9 is a replot of figure 8 with the cross-hatched area indicating the limits for the backscatter from the various models of figures 4 and 5. The upper curve bounding the crosshatched area is the 2 m curve of figure 5 and the lower curve is a composite of the $K\lambda = .04$, $t_p = \delta(t)$ of figure 4 and the 60 m curve of figure 5. Considering that the general observed trend is for the backscatter to decrease with increasing wavelength, the upper region of the crosshatched area is more appropriate for the shorter wavelength and the lower region for the longer wavelengths.

If we define the depth of detectability of a subsurface reflector by signal to noise ratio of 1 (0db), the greatest depth of detectability is found in the case of the two longest wavelengths (20 m and 60 m) in average soil and is about 1 km. In average rock the depth of detectability at the two longest wavelengths is in the range from 100 to 150 m. At 2 m wavelength the models indicate that probably no subsurface reflections would be detectable in either soil or rock.

In considering regions of the lunar surface that might be much smoother than the average surface we could assume that the backscatter is 10 db lower than the lower limit used above. This would increase the depth of detectability at the two lowest frequencies to 1.7 km in average soil and to about 275 m in typical rock. A decrease in the loss tangent by about one third would, at the lowest frequencies, increase the depth in rocks to something like 600 m.

CONCLUSIONS

Based on our estimates and various measured lunar parameters, the expected maximum depth of detectability under typical conditions is about 1 km in soil and about 150 m in rock. The detectability depth will be increased in those regions where the surface roughness is small and/or the propagation losses are small. Factors tending to decrease the detectable depth are an increase in surface roughness, greater than average propagation losses and degradation in the data processing gain.

W. R. Sill

2015-WRS-dmu

Attachment
References

REFERENCES

Beckmann, P. and W. K. Klemperer, Interpretation of the Angular Dependence of Backscattering from the Moon and Venus, Radio Science, 69, 1669, 1965.

Brown, W. E., A Lunar and Planetary Echo Theory, J. Geophys. Res. 65, 3087, 1960.

Brown, W. E., Lunar and Planetary Sciences, JPL Space Programs Summary, 4, No. 37-30, 153, 1964.

Brown, W. E., Radar Studies of the Earth, Proc. IEEE, 57, 612, 1969.

Chung, D. H., W. B. Westphal and G. Simmons, Dielectric Properties of Apollo 11 Lunar Samples and Their Comparison with Earth Minerals, J. Geophys. Res., 75, 6524, 1970.

Collett, L. S. and T. J. Katsube, Electrical Properties of Apollo 11 and 12 Lunar Samples, Paper presented at the Second Annual Lunar Science Conference, Houston, Texas, January 1971.

Evans, J. V. and G. H. Pettengill, The Scattering Behavior of the Moon at Wavelengths of 3.6, 68 and 784 Centimeters, J. Geophys. Res., 68, 423, 1963.

Klemperer, W. K., The Angular Scattering Law for the Moon at 6 Meters Wavelength, J. Geophys. Res., 70, 3798, 1965.

Marcus, A. H., Application of a Statistical Surface Model to Planetary Radar Astronomy, J. Geophys. Res., 74, 4958, 1969.

Strangway, P. W., Moon: Electrical Properties of the Uppermost Layers, Science, 165, 1012, 1969.

Tyler, G. L., Oblique-Scattering Radar Reflectivity of the Lunar Surface: Preliminary Results from Explorer 35, J. Geophys. Res., 73, 7609, 1968.

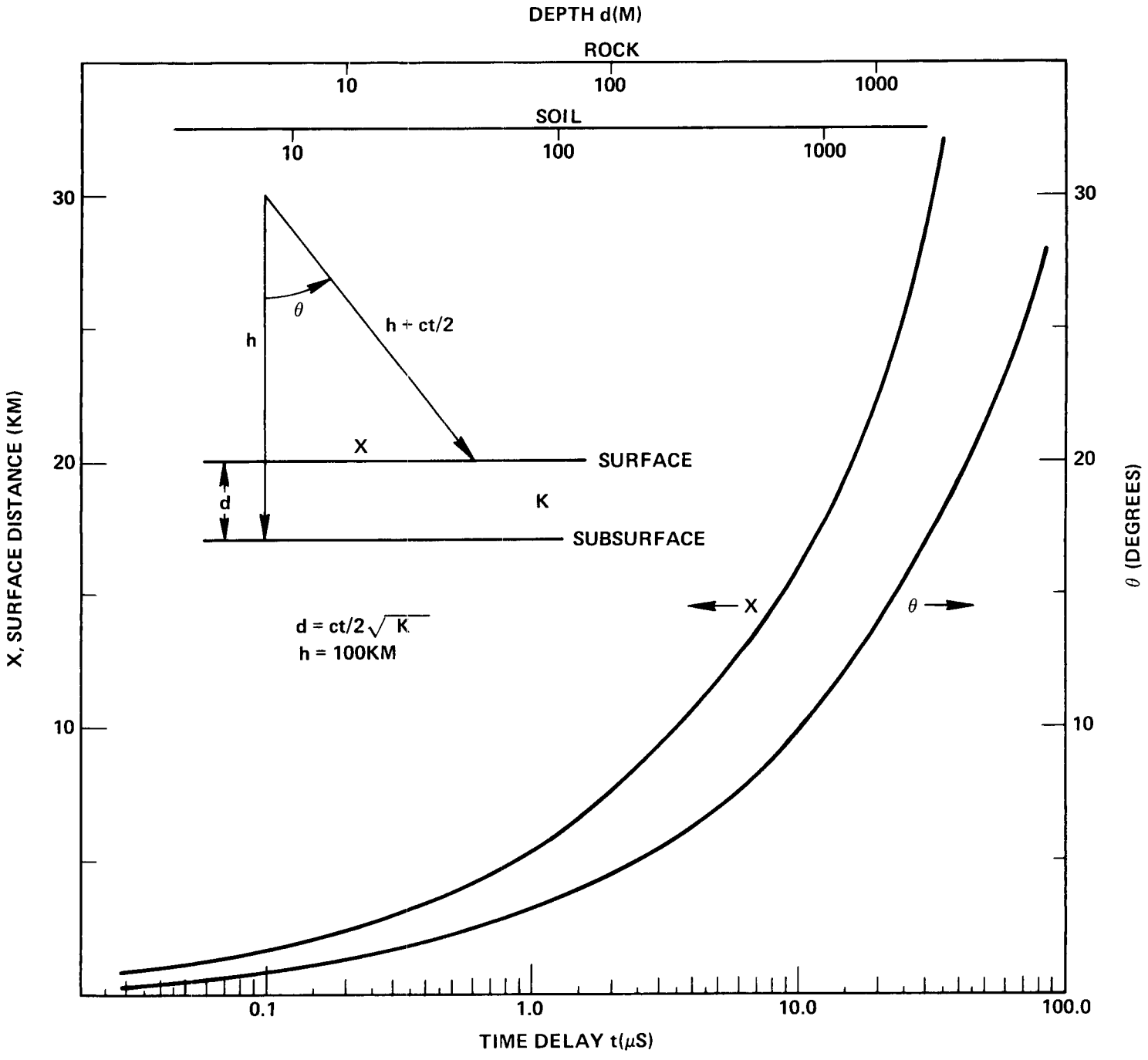

FIGURE 1 - THE HORIZONTAL DISTANCE, AND ANGLE TO A SURFACE SCATTERING POINT AS A FUNCTION OF TIME DELAY AND DEPTH TO AN EQUALLY DELAYED SUBSURFACE REFLECTOR

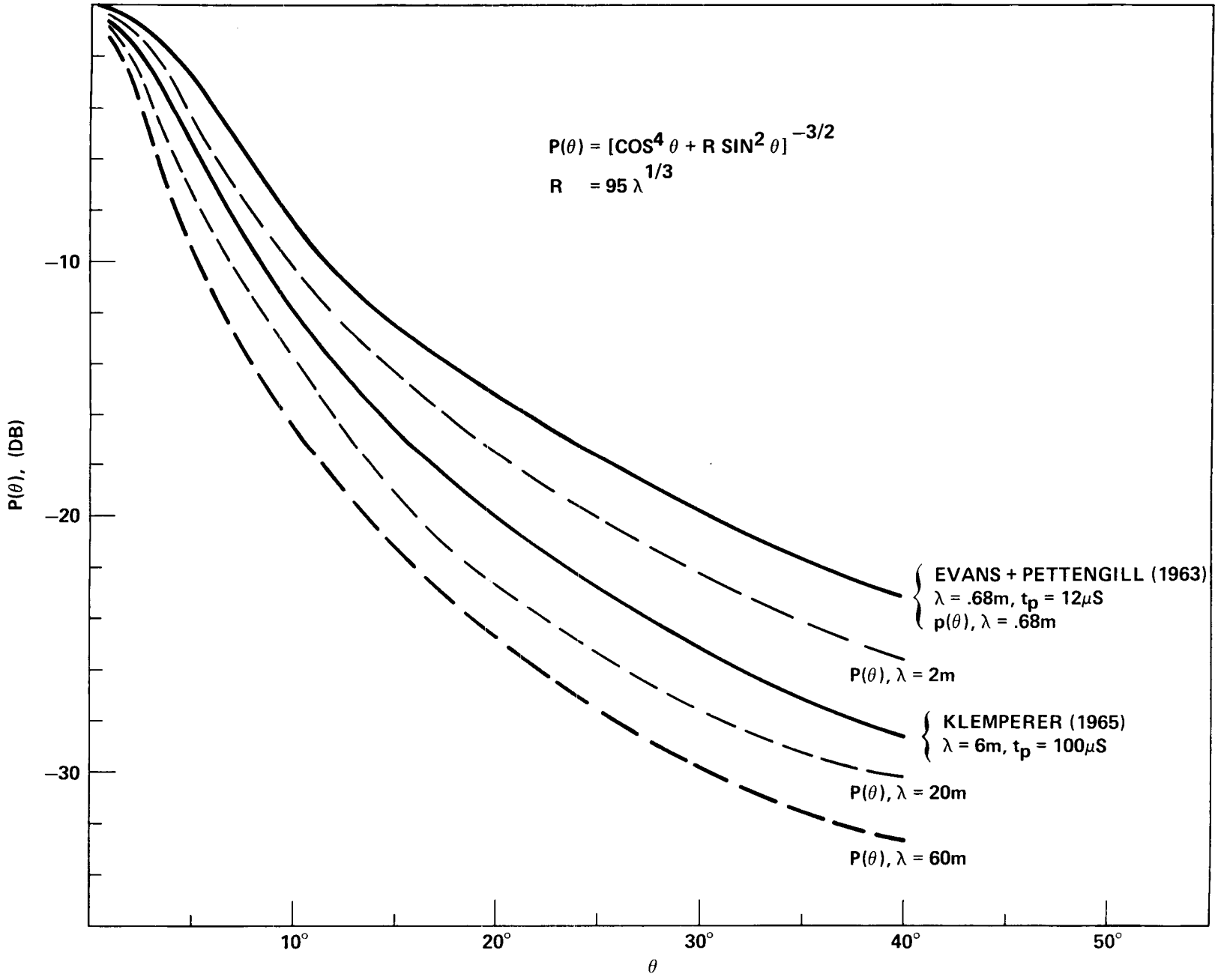

FIGURE 2 - LUNAR BACKSCATTER AS A FUNCTION OF ANGLE OF INCIDENCE FROM EQUATION 1 (BECKMAN AND KLEMPERER, 1965)

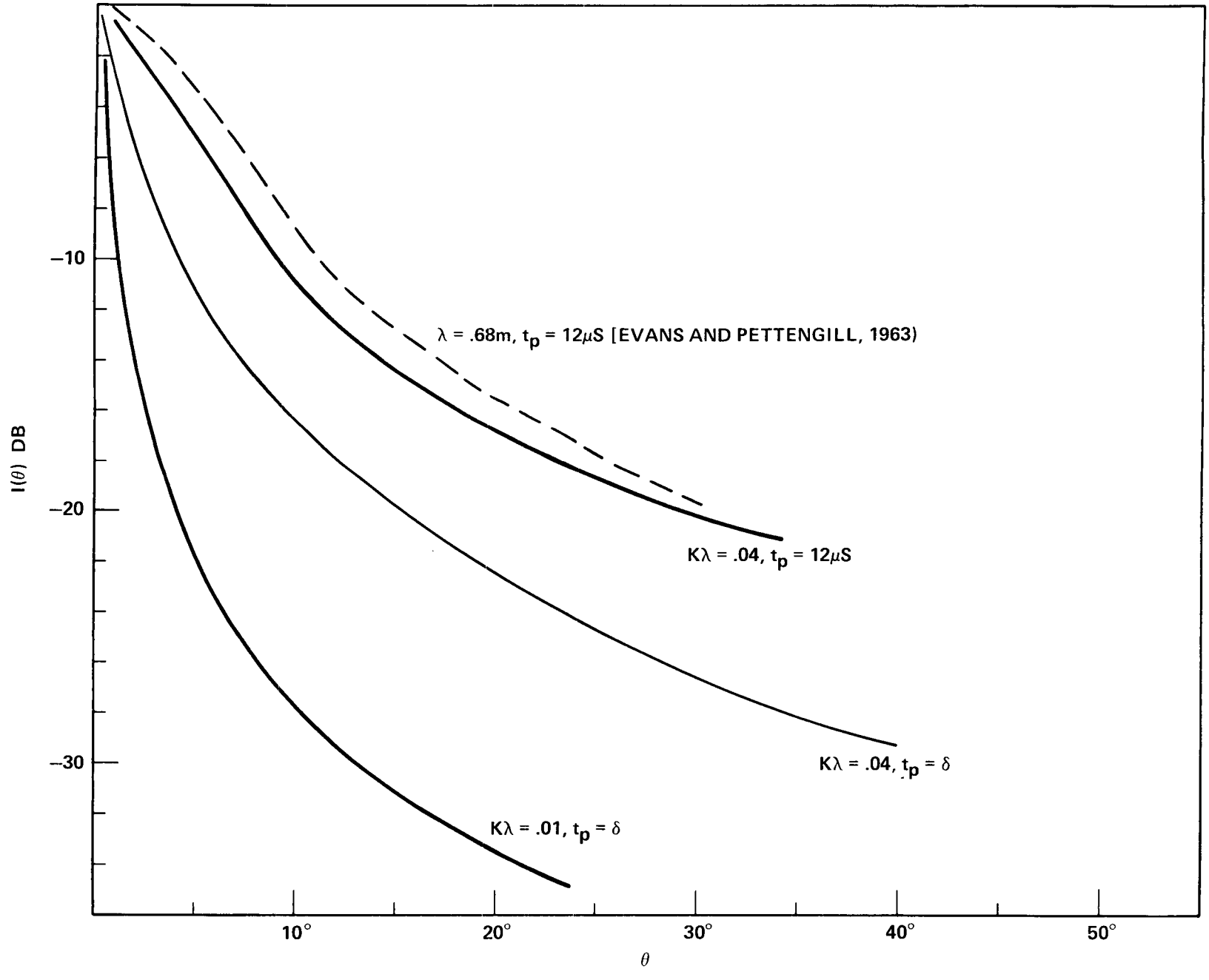

FIGURE 3 - LUNAR BACKSCATTER AND IMPULSE RESPONSE FROM EQUATION 3 (BROWN, 1960 AND 1964)

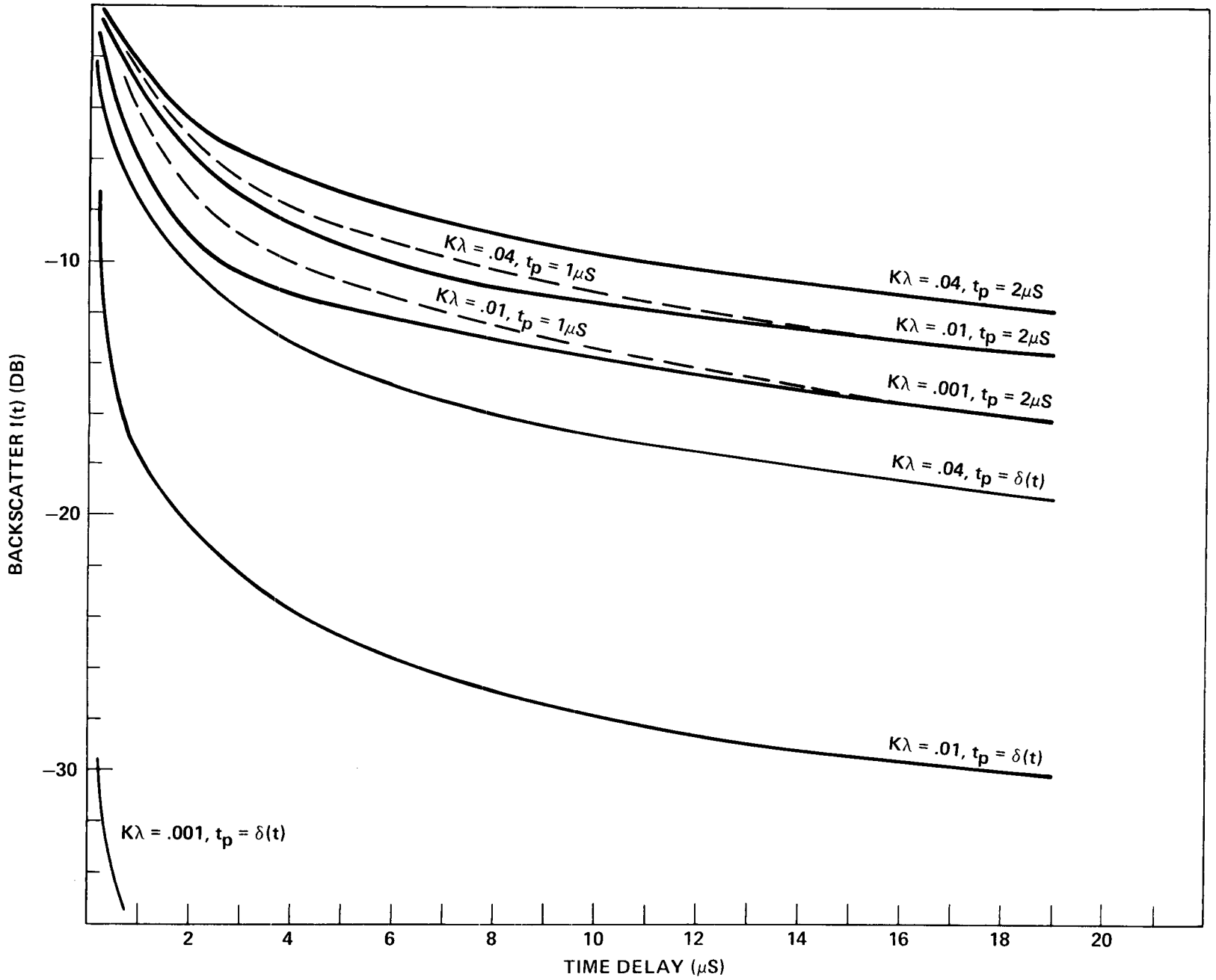

FIGURE 4 - BACKSCATTER FOR LUNAR RADAR SOUNDER GEOMETRY AS A FUNCTION OF TIME DELAY (EQUATION 3)

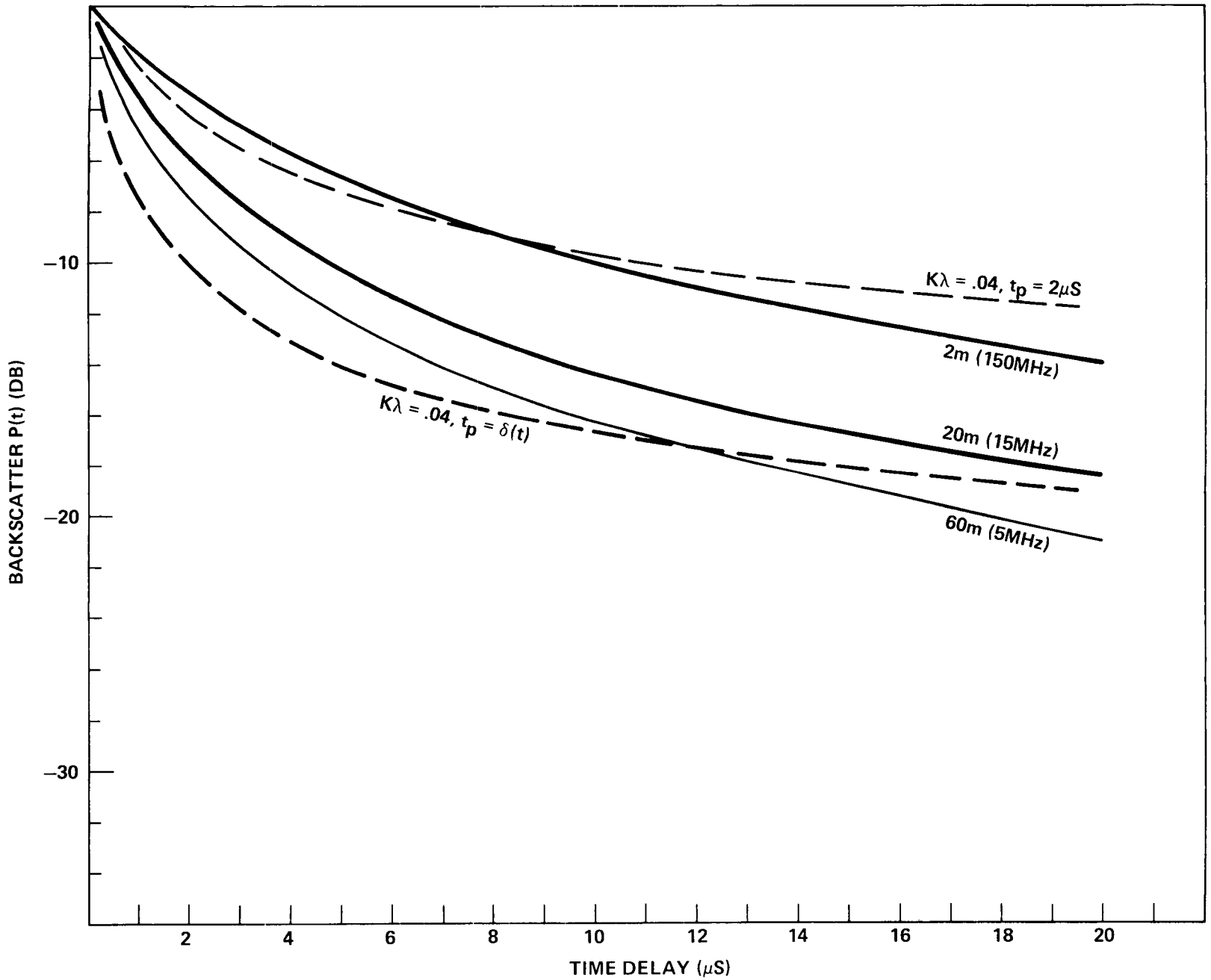

FIGURE 5 - BACKSCATTER FOR LUNAR RADAR SOUNDER GEOMETRY AS A FUNCTION OF TIME DELAY. SOLID CURVES FROM EQUATION 1, DASHED CURVES FROM EQUATION 3

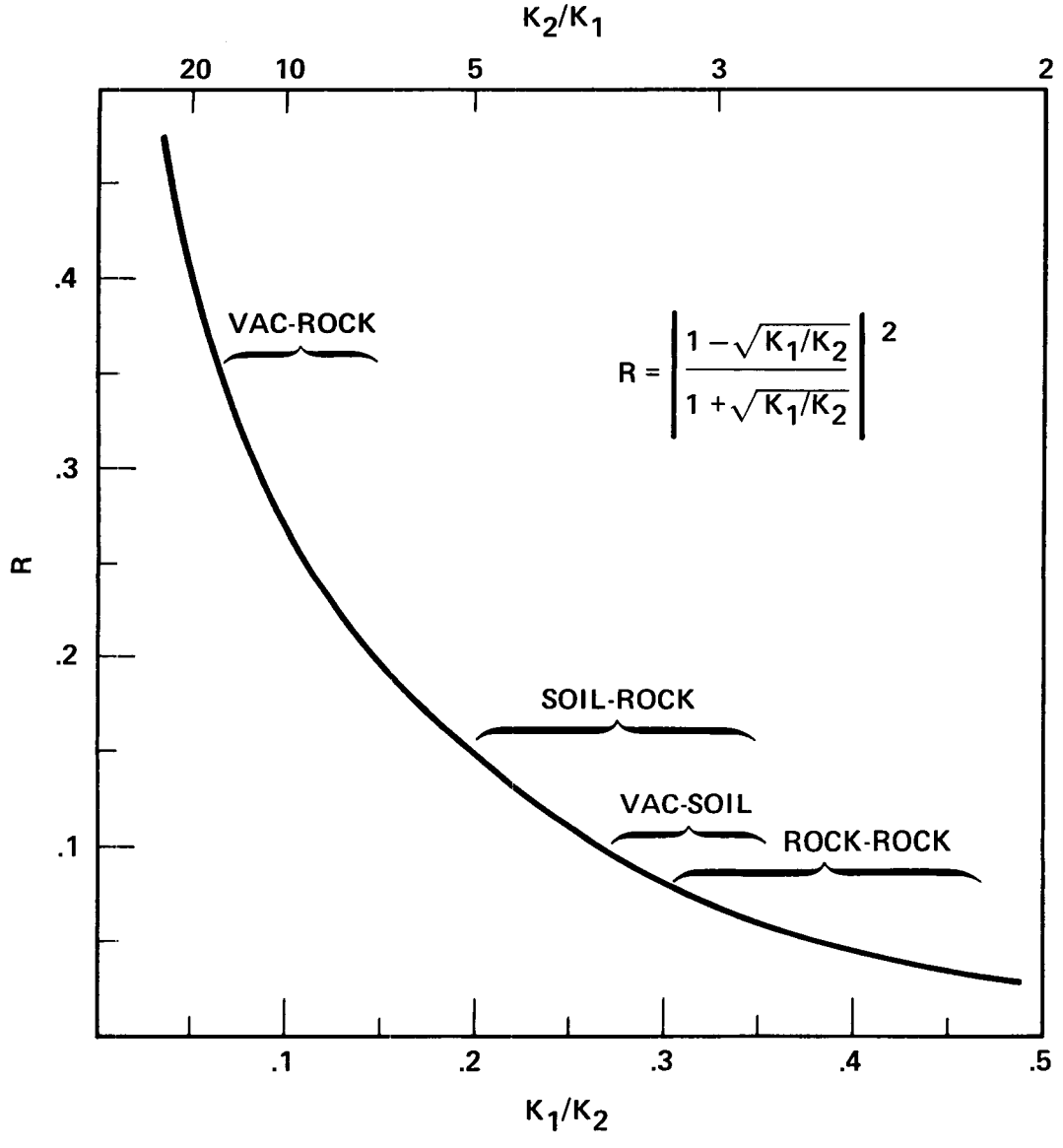

FIGURE 6 - REFLECTION COEFFICIENT (R) AS A FUNCTION OF THE DIELECTRIC CONTRAST (K_1/K_2) ACROSS AN INTERFACE

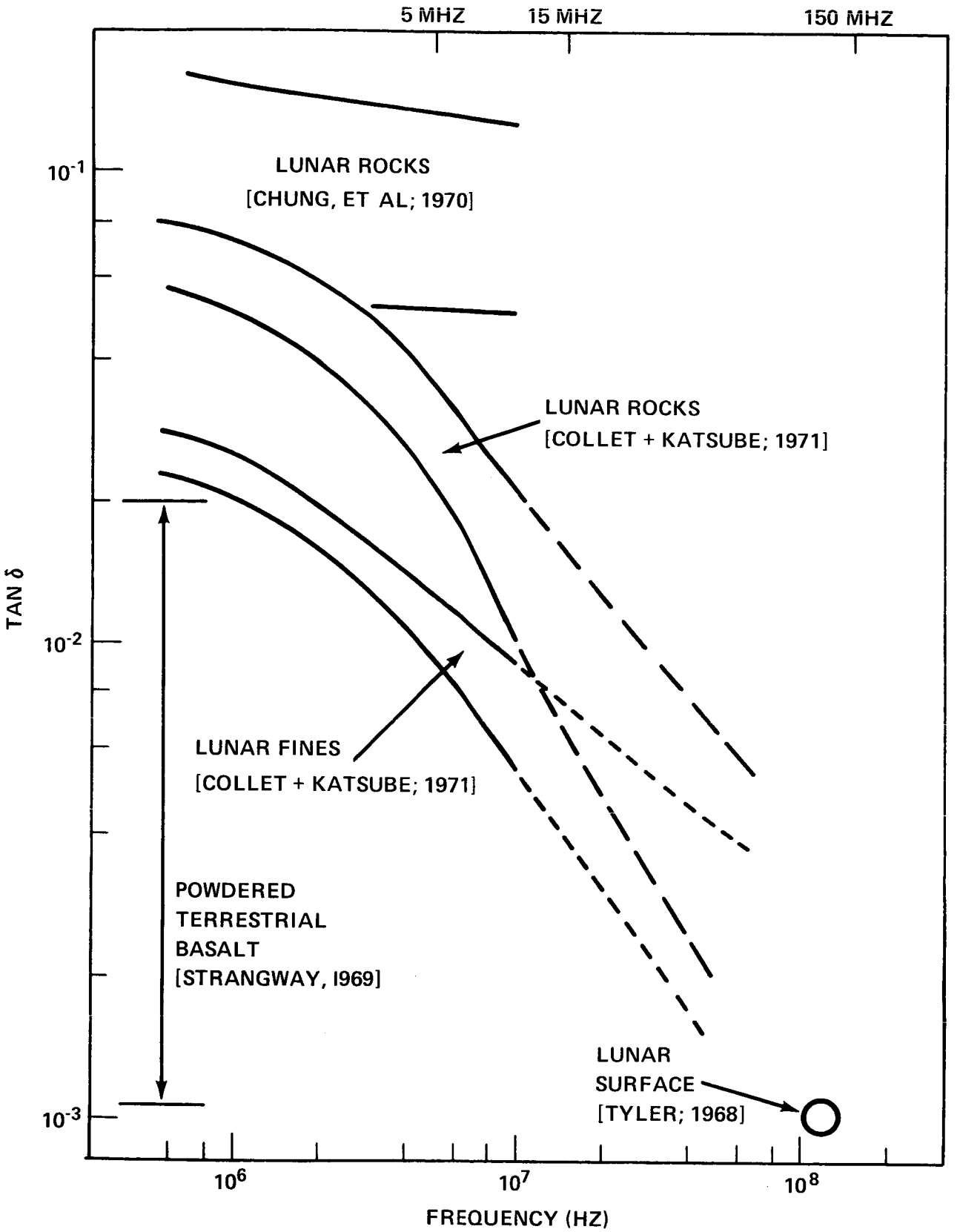

FIGURE 7 - LOSS TANGENT AS A FUNCTION OF FREQUENCY FOR LUNAR AND TERRESTRIAL ROCKS AND FINES

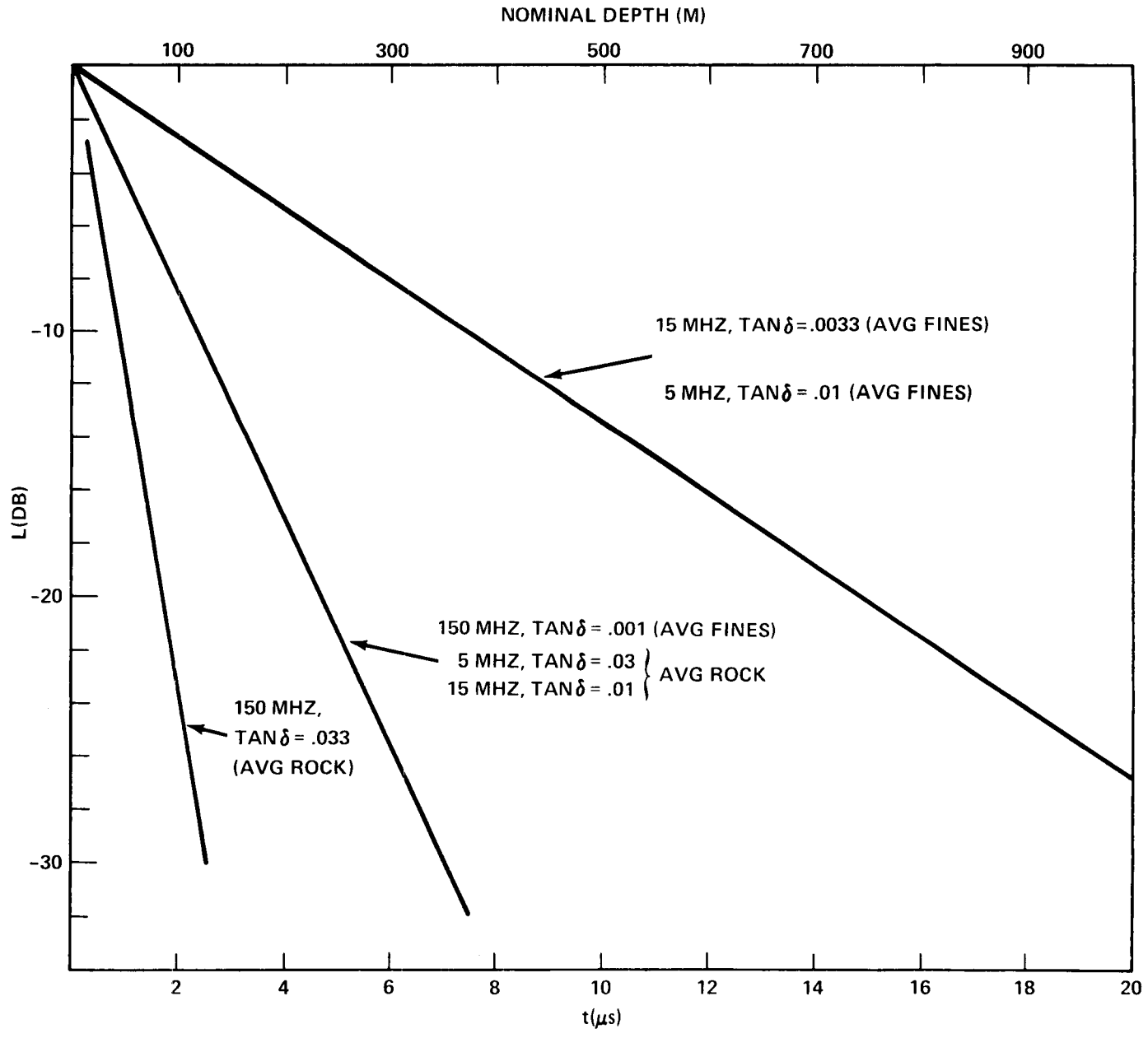

FIGURE 8 - ATTENUATION LOSS FOR LUNAR ROCKS AND FINES AS A FUNCTION OF TIME DELAY

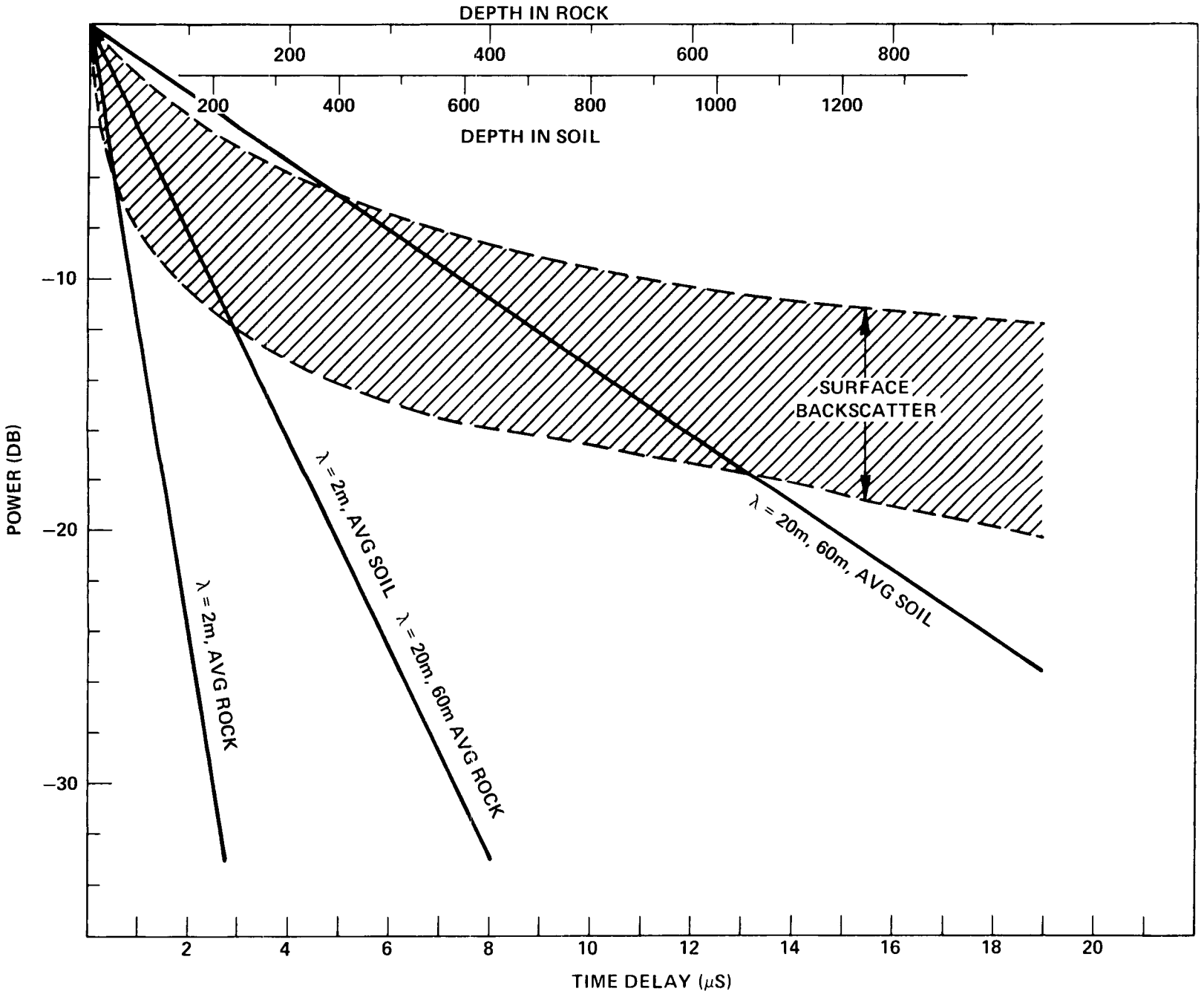

FIGURE 9 - SUBSURFACE ATTENUATION LOSSES AND SURFACE BACKSCATTER AS A FUNCTION OF TIME DELAY AND DEPTH